PASJ: Publ. Astron. Soc. Japan **65**, 121, 2013 December 25

Low-Resolution Spectrum of the Extragalactic Background Light with the AKARI InfraRed Camera

Kohji TSUMURA,[1] Toshio MATSUMOTO,[1,2] Shuji MATSUURA,[1] Itsuki SAKON,[3] and Takehiko WADA[1]
[1]*Department of Space Astronomy and Astrophysics, Institute of Space and Astronautical Science, Japan Aerospace Exploration Agency, 3-1-1 Yoshinodai, Chuo-ku, Sagamihara 252-5210*
tsumura@ir.isas.jaxa.jp
[2]*Institute of Astronomy and Astrophysics, Academia Sinica, No. 1, Roosevelt Rd, Sec. 4, Taipei 10617, Taiwan, R.O.C.*
[3]*Department of Astronomy, Graduate School of Science, The University of Tokyo, 7-3-1 Hongo, Bunkyo-ku, Tokyo 113-0033*

(Received 2013 March 27; accepted 2013 July 25)

Abstract

The Extragalactic Background Light (EBL) as integrated light from outside of our Galaxy includes information about the early universe and the Dark Ages. We analyzed spectral data of the astrophysical diffuse emission obtained with the low-resolution spectroscopy mode on the AKARI Infra-Red Camera (IRC) in the 1.8–5.3 μm wavelength region. Although previous EBL observations in this wavelength region were restricted to observations by DIRBE and IRTS, this study adds a new independent result with negligible contamination of Galactic stars owing to higher sensitivity for point sources. Two other major foreground components, zodiacal light (ZL) and diffuse Galactic light (DGL), were subtracted by taking correlations with ZL brightness estimated by the DIRBE ZL model and with the 100 μm dust thermal emission, respectively. The isotropic emission was obtained as EBL, which shows significant excess over integrated light of galaxies at $< 4\,\mu$m. The obtained EBL is consistent with the previous measurements by IRTS and DIRBE.

Key words: cosmology: diffuse radiation — cosmology: early universe — cosmology: observations — galaxies: intergalactic medium — interplanetary medium

1. Introduction

The Extragalactic Background Light (EBL) is the integrated light of all light sources outside of our Galaxy. At near-infrared (NIR) wavelengths, the dominant physical process for the generation of photons is thought to be nucleosynthesis in stars. EBL contains the accumulated history from the first stars of the universe to stars of the present days. Galaxy counts provide necessarily lower limits to EBL, although unresolved or faint emission sources may also contribute to EBL. One possible and important faint source is the first stars of the universe, which reionized the universe. Since individual detection of the first stars is extremely difficult even with JWST, the excess background over the integrated light of galaxies has been searched for. Separating EBL from foreground emission is very difficult due to its diffuse, extended nature. The largest uncertainty comes from removal of the dominant foreground, the zodiacal light (ZL), which is the scattered sunlight by interplanetary dust (IPD) at $< 3.5\,\mu$m, and thermal emission from the same IPD at $> 3.5\,\mu$m.

In order to determine the total EBL brightness, the absolute measurement of sky brightness from space is inevitable to avoid strong airglow emission. The Diffuse Infrared Background Explorer (DIRBE) on the Cosmic Background Explorer (COBE) (Hauser et al. 1998; Cambŕesy et al. 2001) and the Near-Infrared Spectrometer (NIRS) on the Infrared Telescope in Space (IRTS) (Matsumoto et al. 2005) indicate that the total EBL brightness at NIR after subtraction of ZL and other foregrounds significantly exceeds the brightness determined from deep galaxy number counts (Domínguez et al. 2011). However, EBL derived from absolute measurements depends critically on the choice of ZL models (Kelsall et al. 1998; Wright 1998). EBL in optical bands has been measured by Bernstein (2007), Matsuoka et al. (2011), and Mattila et al. (2011); however, their results are controversial. Beside uncertainty of the ZL model, it has been claimed that observations of TeV-γ blazars favor low-level EBL at NIR (Dwek et al. 2005b; Aharonian et al. 2006, 2007; Mazin & Raue 2007; Raue et al. 2009). Furthermore, it has been pointed out that a vast formation rate during the first star formation era is needed, if we attribute the origin of this excess emission to the first stars (Madau & Silk 2005).

In order to confirm the origin of excess emission, new space observations have been desired. Unfortunately, Spitzer was unable to perform absolute measurements of the surface brightness of the sky because of the lack of a cold shutter (Fazio et al. 2004a). Here, we present the new result of EBL observations with AKARI InfraRed Camera (IRC). One advantage of AKARI/IRC observations is its detection limit for point sources ($m_K \sim 19$), which is much deeper than that of COBE/DIRBE and IRTS/NIRS owing to the large-aperture telescope. This makes the contribution of Galactic stars to the background radiation almost negligible, and subtraction of the foreground emission more reliable.

This paper is organized as follows. In section 2, we describe the data reduction. In section 3, we describe our method for subtracting foreground emissions, and the resultant EBL spectrum is shown in section 4. Discussions and implications of our data are given in section 5. There are two companion papers that describe the spectra of the infrared diffuse foregrounds;

the data-reduction method and ZL is described in Tsumura et al. (2013a, hereafter Paper I) and the Diffuse Galactic Light (DGL) in Tsumura et al. (2013b, hereafter Paper II). The results given in Papers I and II were used in the present work (Paper III) for foreground subtraction.

2. Data Selection and Reduction

AKARI is the first Japanese infrared astronomical satellite, launched on 2006 February, equipped with a cryogenically cooled telescope of 68.5 cm aperture diameter (Murakami et al. 2007). IRC is one of two astronomical instruments of AKARI, which covers the 1.8–5.3 μm wavelength region with a 512 × 412 InSb detector array in the NIR channel[1] (Onaka et al. 2007). It provides low-resolution ($\lambda/\Delta\lambda \sim 20$) slit spectroscopy for diffuse radiation by a prism[2] (Ohyama et al. 2007).

See Paper I for the details concerning the data selection and reduction. According to our criteria of data selection for diffuse background analysis (Paper I), a total number of 278 diffuse spectra toward randomly distributed sky directions in wide ranges of ecliptic and Galactic coordinates were selected. A filter wheel of the IRC instrument has a dark position to measure the dark current, while the cold shutter of Spitzer has not been operated in orbit (Fazio et al. 2004a). The uncertainty due to dark-current subtraction is estimated to be $< 3\,\mathrm{nW\,m^{-2}\,sr^{-1}}$ at 2 μm (Tsumura & Wada 2011).

Point sources brighter than $m_K(\mathrm{Vega}) = 19$ were detected on the slit, and masked for deriving the diffuse spectrum. It was confirmed that the brightness due to unresolved Galactic stars under this detection limit is negligible ($< 0.5\%$ of the sky brightness at 2.2 μm) by a Milky Way star count model, TRILEGAL (Girardi et al. 2005). This is a great advantage to the previous measurements by DIRBE and IRTS, because the integrated light from unresolved Galactic stars for those measurements is not negligible. For example, in the IRTS case, the limiting magnitude for removing point sources was 10.45 mag at 2.24 μm, and the contribution of the integrated light from unresolved Galactic stars under this limiting magnitude was $\sim 10\%$ of the observed sky brightness at high ecliptic latitude (Matsumoto et al. 2005), which was subtracted by the SKY model for Galactic point sources (Cohen 1994). The contamination from unresolved Galactic stars for the DIRBE measurement was $\sim 25\%$ at 2.2 μm (Hauser et al. 1998), which is greater than that of IRTS owing to the worse detection limit of DIRBE.

The obtained diffuse sky spectrum includes ZL, DGL, and EBL, i.e.,

$$SKY_i(\lambda) = ZL_i(\lambda) + DGL_i(\lambda) + EBL_i(\lambda), \quad (1)$$

where i is the data index. The cumulative brightness contributed by unresolved galaxies can be estimated by the deep galaxy counts, being $< 4\,\mathrm{nW\,m^{-2}\,sr^{-1}}$ at the K band in the case of a limiting magnitude of $m_K = 19$ (Keenan et al. 2010), which is included in EBL. Figure 1 shows an example of the sky spectrum at NEP with each foreground component estimated by the methods introduced in Paper I and Paper II.

[1] IRC has two other channels covering 5.8–14.1 μm in the MIR-S channel and 12.4–26.5 μm in the MIR-L channel.

[2] High-resolution spectroscopy ($\lambda/\Delta\lambda \sim 120$) with a grism is also available.

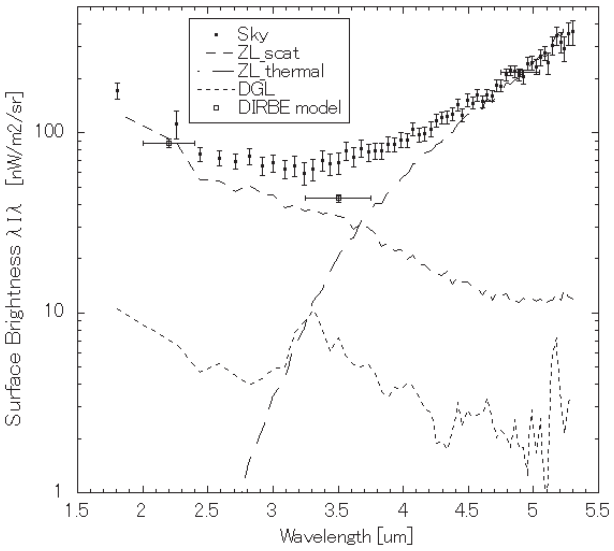

Fig. 1. Example of the sky spectrum at NEP with foreground components. The solid circles indicate the sky spectrum in our dataset obtained by AKARI IRC. The broken line and the dashed line indicate the ZL spectrum (scattered sunlight component and thermal emission component) scaling to the brightness from the DIRBE ZL model (open squares); the dotted line indicates the DGL spectrum.

In the next section, we summarize the methods of foreground subtraction, which are essential to derive EBL.

3. Subtraction of Foregrounds

3.1. Estimation of Diffuse Galactic Light

The method used to estimate the DGL spectrum in our dataset is developed in Paper II. This method can be separated into two stages: the first is to derive the spectral shape of DGL as a template [$DGL_{\mathrm{temp}}(\lambda)$] by a correlation to the 100 μm dust thermal emission, $I^{100\mu\mathrm{m}}$ (Schlegel et al. 1998); the next is to scale this DGL template spectrum by using the relation between $I^{100\mu\mathrm{m}}$ and the 3.3 μm PAH band emission, $E_{3.3}$, i.e.,

$$DGL_i(\lambda) = E_{3.3}(I_i^{100\mu\mathrm{m}}) \times DGL_{\mathrm{temp}}(\lambda). \quad (2)$$

The key point in the first step is that only DGL has any correlation to the 100 μm emission from interstellar dust. Thus, $SKY_i(\lambda) - ZL_i(\lambda)$ at each wavelength is correlated to the dust emission at 100 μm, and this correlated component can be derived as DGL from the sky spectrum. Here, $ZL_i(\lambda)$ is modeled in Paper I and summarized in the next subsection. The derived DGL spectrum has a distinct PAH band feature at 3.3 μm, as shown in figure 1.

The 3.3 μm PAH band feature is distinctive at the bottom of the sky spectrum in our dataset at low Galactic latitude regions ($|\ b\ | < 15°$), and a good correlation between the 100 μm dust thermal emission, $I^{100\mu\mathrm{m}}$, and the 3.3 μm PAH band emission, $E_{3.3}$, was confirmed in Paper II. Assuming that the spectral shape of the template DGL spectrum is isotropic at low Galactic latitude regions, the DGL spectrum at each field, $DGL_i(\lambda)$, is derived by scaling the DGL template spectrum using the relation $E_{3.3}(I^{100\mu\mathrm{m}})$ between the PAH band intensity and the dust thermal emission. In the low DGL

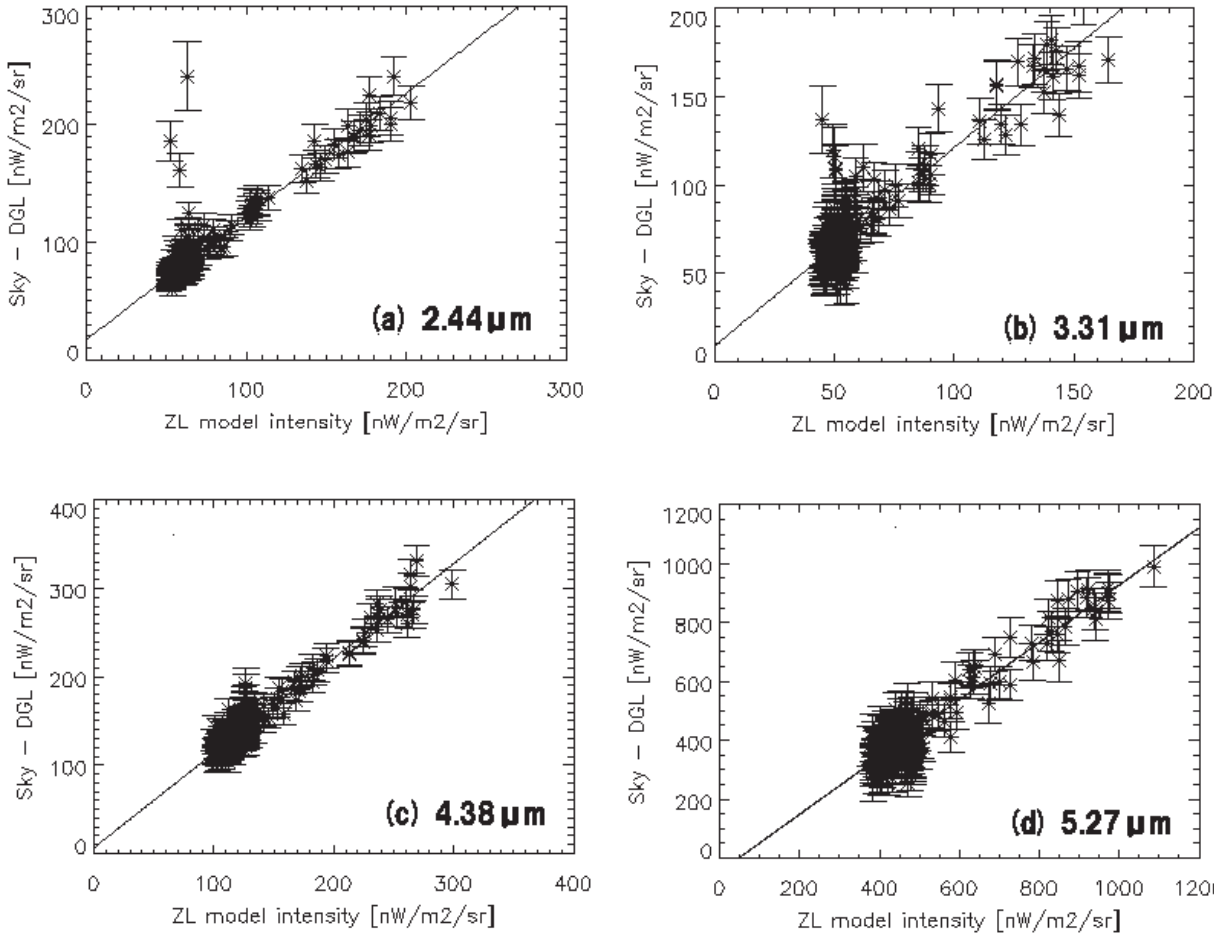

Fig. 2. Examples of correlation between $SKY_i(\lambda) - DGL_i(\lambda)$ and $ZL_i(\lambda)$ from equation (3) at (a) 2.44 μm, (b) 3.31 μm, (c) 4.38 μm, and (d) 5.27 μm. The best-fit lines are also shown, and the error bars in these plots include both statistic random error and the calibration error.

region at the high Galactic latitude ($|\, b \,| > 30°$) used in this study, this relation can be approximated as a linear relation, $E_{3.3}(I^{100\mu m}) \propto I^{100\mu m}$.

3.2. Estimation of Zodiacal Light

The method to estimate the ZL spectrum in our dataset is developed in Paper I. Similar to the method of DGL, the method of ZL estimation has also two stages: deriving the template ZL spectrum, and scaling it. The template ZL spectrum is derived by differencing the DGL-subtracted spectra at the ecliptic plane (ZL strongest region) and that at NEP (ZL weakest region), because only ZL depends on the ecliptic latitude, and the isotropic EBL is removed by differencing. In the wavelength range of this study (1.8–5.3 μm), ZL includes both the scattered sunlight component (~ 5800 K) and the thermal emission component (~ 300 K). We confirmed in Paper I that the spectral shape of each component does not depend on location, while their brightness ratio depends on location. Therefore, the template spectrum of each component was derived separately [$ZL^{\rm scat}_{\rm temp}(\lambda)$ and $ZL^{\rm thermal}_{\rm temp}(\lambda)$]. The scalings of these template ZL spectra are based on the DIRBE ZL model (Kelsall et al. 1998), providing the model ZL intensities at 2.2 μm and 4.9 μm ($DIRBE_i^{2.2\mu m}$ and $DIRBE_i^{4.9\mu m}$) for each field at any observed time.

$$ZL_i(\lambda) = ZL_i^{\rm scat}(\lambda) + ZL_i^{\rm thermal}(\lambda), \quad (3)$$

$$ZL_i^{\rm scat}(\lambda) = DIRBE_i^{2.2\mu m} \times ZL^{\rm scat}_{\rm temp}(\lambda), \quad (4)$$

$$ZL_i^{\rm thermal}(\lambda) = [DIRBE_i^{4.9\mu m} - ZL_i^{\rm scat}(4.9\,\mu{\rm m})] \times ZL^{\rm thermal}_{\rm temp}(\lambda). \quad (5)$$

The estimated ZL brightness at 3.5 μm by this method is consistent with that from the DIRBE ZL model. The model uncertainty of the DIRBE ZL model is 6 nW m^{-2} sr^{-1} at 2.2 μm, 2.1 nW m^{-2} sr^{-1} at 3.5 μm, and 5.9 nW m^{-2} sr^{-1} at 4.9 μm (Kelsall et al. 1998).

3.3. Correlation Analysis

To derive the isotropic component, we employed a correlation analysis. First, data at the Galactic plane ($|\, b \,| < 30°$) were removed from this correlation analysis so as to avoid contamination from the high DGL. Thus, the remaining dataset has a small DGL component, which is estimated by equation (2). Since the DGL-subtracted spectra have two components (ZL and EBL), the correlation between $SKY_i(\lambda) - DGL_i(\lambda)$ and $ZL_i(\lambda)$ from equation (3) was investigated at each wavelength,

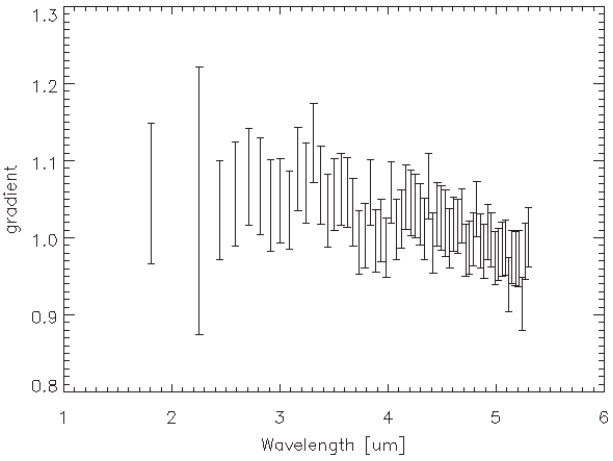

Fig. 3. Gradients of the correlation between $SKY_i(\lambda) - DGL_i(\lambda)$ and $ZL_i(\lambda)$ shown in figure 2. This is used as a correction factor of ZL, $C(\lambda)$. The large error bars, especially at short wavelengths, are dominated by the calibration error.

$$SKY_i(\lambda) - DGL_i(\lambda) = C(\lambda) \times ZL_i(\lambda) + EBL(\lambda). \quad (6)$$

Two fitting parameters [$C(\lambda)$ and $EBL(\lambda)$] are obtained by the correlation, and the gradients of these correlations, $C(\lambda)$, give us a correction of our ZL estimation; y-intercepts indicate the isotopic EBL. Examples of correlations at some wavelengths are shown in figure 2. The best-fit lines in figure 2 were obtained after 3σ clipping for outlier rejection, and their gradients, $C(\lambda)$, are shown in figure 3. Fairly good correlations can be seen, and the gradient $C(\lambda)$ is basically consistent with unity within the error bars, indicating that the DIRBE ZL model is consistent with our data set. However, the gradients at short wavelengths ($< 3.5\,\mu$m) are larger than unity by $\sim 5\%$, indicating that the DIRBE ZL model underestimates the ZL intensity at these wavelengths. This trend is consistent with the fact that the estimated ZL brightness values by the DIRBE ZL model are smaller than other models by 5%–8% at 1.25 μm and 11%–14% at 2.2 μm (Kelsall et al. 1998).

The dataset used in this study includes two types of errors: the statistical random error and the calibration error. The statistic error includes the instrumental noise, the uncertainty of the ZL estimation, and the uncertainty of the DGL estimation. As described in Paper I, the calibration error [$Err^{\rm cal}(\lambda)$] is estimated to be 8% at 1.8 μm, 16% at 2.2 μm, and $< 5\%$ at $> 2.5\,\mu$m. The calibration error is larger than the statistical error at $< 3.5\,\mu$m. Since the propagations of these errors are different, these two errors were separately investigated in this correlation analysis. First, the correlation analysis was conducted with only the statistical random errors, and EBL at each wavelength was obtained as y-intersects with errors, $EBL(\lambda) \pm Err1(\lambda)$. Errors owing to the calibration is estimated as $Err2(\lambda) = EBL(\lambda) \times Err^{\rm cal}(\lambda)$. Then, these two types of errors were added to obtain the total error, $Err^{\rm total}(\lambda) = \sqrt{Err1(\lambda)^2 + Err2(\lambda)^2}$.

4. Result

Figure 4 shows the resultant EBL spectrum from our AKARI dataset along with various previous results. The Galactic and ecliptic latitude dependences of the obtained EBL were checked, as shown in figure 5; the obtained EBL brightness is basically confirmed to be isotropic.

Our spectrum by AKARI/IRC clearly indicates the excess over the integrated light of galaxies, and is basically consistent with the revised IRTS result (T. Matsumoto et al. in preparation) and DIRBE results (Cambrésy et al. 2001; Levenson et al. 2007). At wavelengths shorter than 3 μm, the AKARI result shows a little lower brightness than the IRTS result. This difference could be attributed to the difference of the detection limits for point sources. At the K band, the limiting magnitude of the AKARI dataset for removing point sources is 19 mag, while that of IRTS is 10.5 mag. The difference of the integrated light of unresolved galaxies owing to this limiting magnitude difference is estimated to be $\sim 5\,{\rm nW\,m^{-2}\,sr^{-1}}$ (Keenan et al. 2010), which explains the difference of the EBL brightness.

There is a gap in our result between 3.0 μm and 3.5 μm due to the difficulty of modeling the foregrounds in this wavelength region. As shown in figure 1, the diffuse sky brightness in this wavelength range includes all three of foreground components (scattered sunlight of IPD, thermal emission from IPD, and DGL with the 3.3 μm PAH band) with similar fractions, which makes the foreground modeling difficult. One possible explanation for the gap at around 3.3 μm is an overestimate of the 3.3 μm PAH band intensity. In fact, if we estimate DGL without the PAH band, the gap disappears and the EBL spectrum becomes smooth. This suggests that the correlation between the PAH band emission and the 100 μm intensity at high Galactic latitude is fairly weaker than that at low Galactic latitude. As described in Paper II, the correlation between the PAH band and the 100 μm intensity is confirmed only at $| b | < 15^\circ$, and the DGL spectrum is estimated by extrapolation of this correlation to the higher Galactic latitude regions in our method. However, this assumption is obviously too simple. For example, the UV radiation field at high Galactic latitude is weaker than that at the Galactic plane (Seon et al. 2011), therefore the PAH molecules are less excited at high Galactic latitude than the Galactic plane. This consideration indicates that the gap around 3.3 μm could not be EBL origin but Galactic origin.

We obtained a new spectral result of EBL at $> 4\,\mu$m, and cannot confirm the excess over the integrated light of galaxies due to the large error bars. In addition, our result contradicts the high EBL brightness at 4.9 μm by Arendt and Dwek (2003), but this data point is highly uncertain, since it is not an observed value, but an estimated value from EBL at 1.25, 2.2, 3.5, and 100 μm.

5. Discussion

In section 4, we found NIR EBL observed with AKARI to be fairly consistent with previous observations by COBE/DIRBE and IRTS/NIRS. How can we understand the excess of EBL from the integrated light of galaxies at $< 4\,\mu$m?

At first we examine the possible origin in the solar system. If there is an isotropic component in ZL, it cannot be subtracted by the correlation method in our study. One candidate of an isotropic ZL component is a dust shell contingent on Earth, but such a dense dust shell around Earth must have been detected

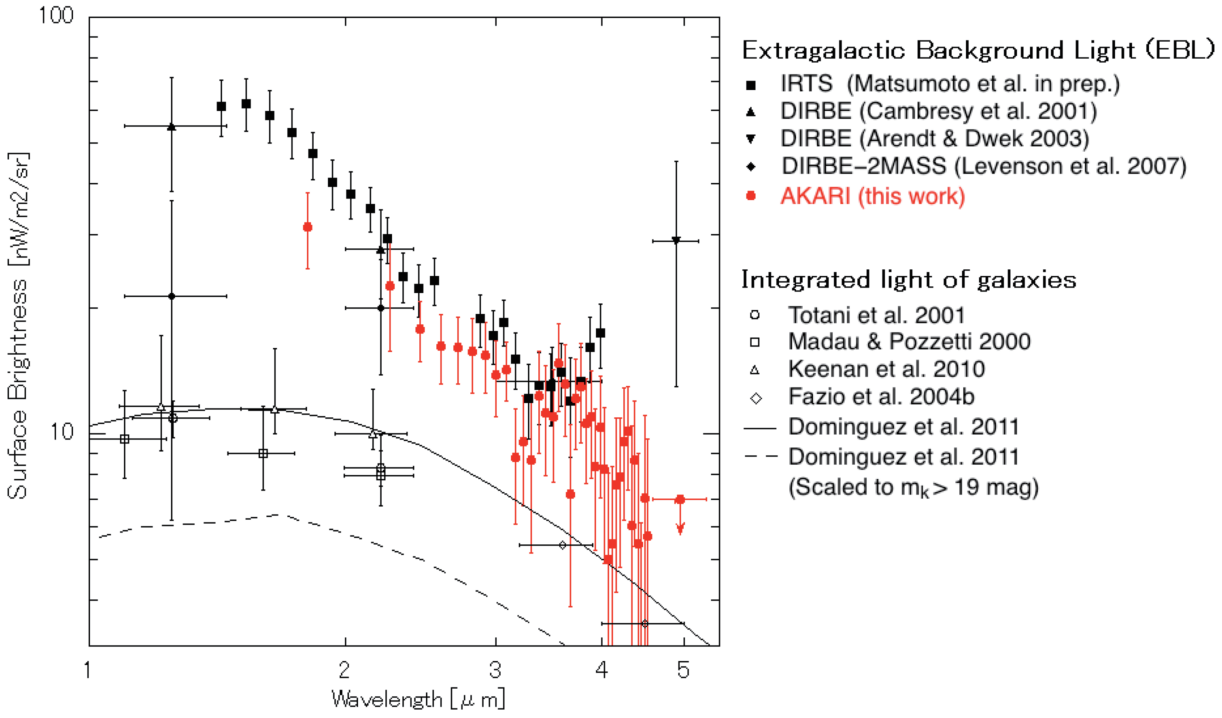

Fig. 4. Spectra of EBL and integrated light of galaxies. Filled plots show EBL by various direct photometry from space, including this study; open plots shows the integrated light of galaxies by deep observations. Horizontal bars show the band widths of wide-band data. The solid curve shows a model spectrum of the integrated light of galaxies based on the observed evolution of the rest-frame K-band galaxy luminosity function up to redshift 4 (Domínguez et al. 2011); the broken curve shows a scaled version of it in the case of AKARI's detection limit of point sources ($m_K = 19$).

already, if it exists. An isotropic diffuse background from the Oort cloud could be another candidate. However, the very blue spectrum toward 1 μm cannot be generated by thermal emission from very cold dust (< 30 K) at the Oort cloud. Scattered sunlight by the Oort cloud is also negligible because sunlight at $\sim 10^4$–10^5 au is very weak.

The second possibility is Galactic origin. There may exist numerous faint stars in the Galactic halo that cause an isotropic background. However, the negative detection of an extended halo in external galaxies was reported by Uemizu et al. (1998). Furthermore, the observed excess emission, ~ 23 mag arcsec^{-2} at the H-band, can be easily detected for the external galaxies with HST/NICMOS (Thompson et al. 2007a, 2007b), but no detection has been reported yet. These considerations support the idea that the observed excess emission is of extragalactic origin.

The observations of TeV-γ blazars are another problem for the extragalactic origin, since a high-level NIR EBL makes intergalactic space opaque for TeV-γ photons (Dwek et al. 2005b; Aharonian et al. 2006, 2007; Mazin & Raue 2007; Raue et al. 2009). However, recent discoveries of high-redshift ($z > 0.6$) TeV-γ blazars (Furniss et al. 2013) contradict with the above standard scenario, and it requires a new physical process. One idea is that cosmic rays produced by blazars can cross cosmological distances, and interact with NIR photons relatively close to Earth, generating secondary TeV γ-ray photons (Essey & Kusenko 2010). Another possible idea is that if TeV γ-ray photons are converted into Axion-like particles (ALPs), they would then be regenerated to TeV γ-ray photons in our Galaxy. In this case, TeV γ-ray photons should not suffer absorption effects while they propagate as ALPs (Sánchez-Conde et al. 2009). If these processes work well, TeV γ-ray and EBL observations can coexist.

Spatial fluctuations of EBL were observed at 2.4, 3.2, and 4.1 μm by AKARI IRC imaging data (Matsumoto et al. 2011) and at 3.6 and 4.5 μm by Spitzer IRAC imaging data (Kashlinsky et al. 2005, 2007, 2012) in order to avoid uncertainty of the ZL model, since ZL is known to be spatially smooth (Pyo et al. 2012). The observed fluctuations are consistent with each other, and show significantly large fluctuations at an angular scale larger than 100″, which cannot be explained by known foreground emission. The ratio of the EBL fluctuating power at $> 100''$ scale (Matsumoto et al. 2011) to the absolute EBL spectrum (our result) can be obtained from the same instrument during the same season; we obtained $\delta I/I = 0.014$ at 2.4 μm, 0.012 at 3.2 μm, and 0.0063 at 4.1 μm. We also compared our EBL spectrum with the EBL fluctuating power at $> 100''$ scale obtained by Spitzer (Kashlinsky et al. 2012), obtaining $\delta I/I = 0.0064$ at both 3.6 μm and 4.5 μm. These results are consistent with $\delta I/I \sim 0.01$ at any wavelengths from a theoretical estimation to predict the EBL fluctuations by the structure formation during the early universe (Fernandez et al. 2010), supporting that both of the observed EBL spectrum excess and fluctuation have the same origin.

One notable candidate concerning the origin of the EBL excess and fluctuation is first stars of the universe (Santos et al. 2002; Salvaterra & Ferrara 2003; Cooray & Yoshida 2004; Dwek et al. 2005a; Madau & Silk 2005; Mii & Totani

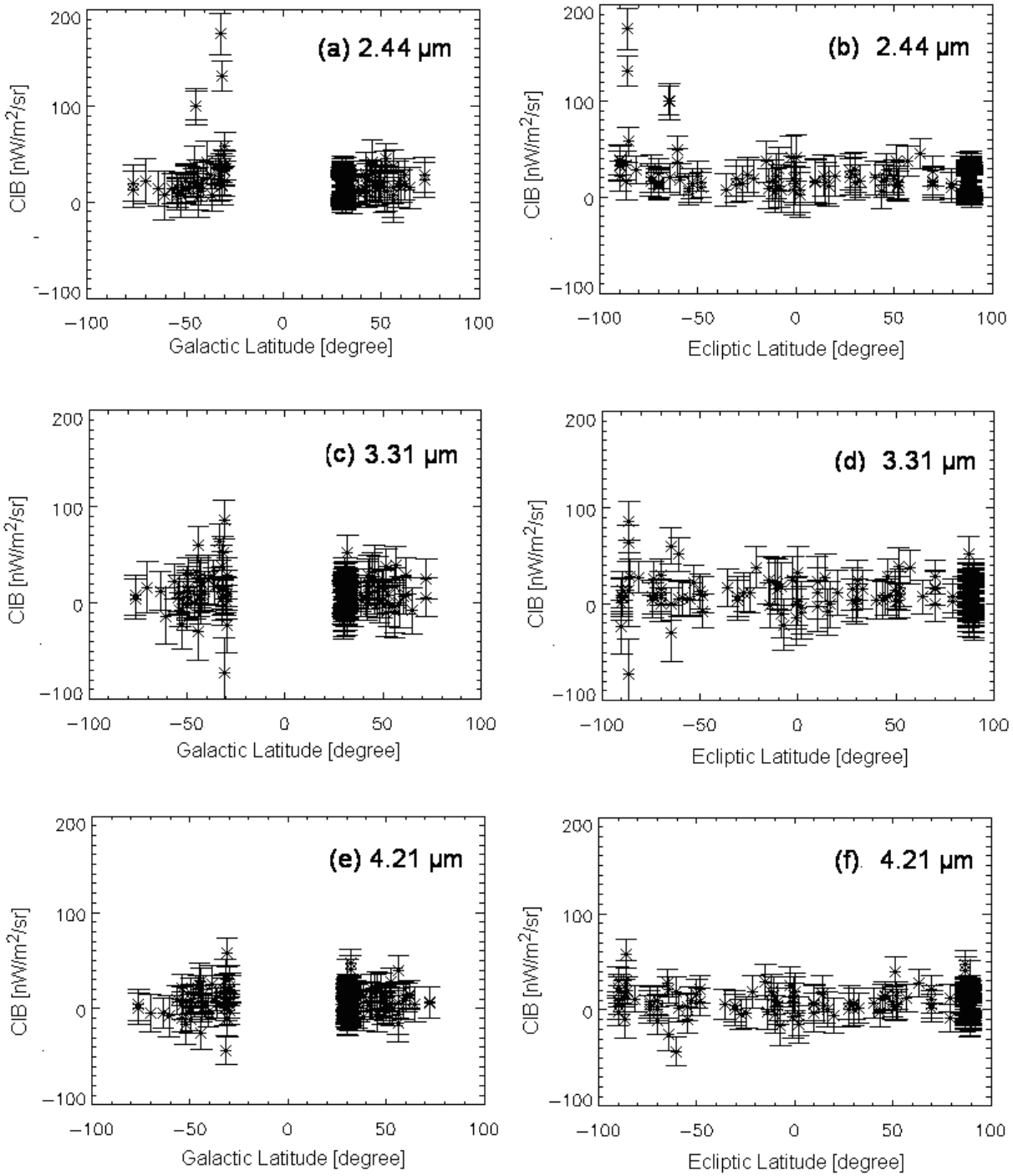

Fig. 5. Galactic latitude (a, c, e) and ecliptic latitude (b, d, f) dependence of EBL at 2.25 μm (a, b), 3.31 μm (c, d), and 4.21 μm (e, f). The error bars in this plot include only the statistic error [$Err1(\lambda)$].

2005; Fernandez & Komatsu 2006; Fernandez et al. 2010). Our spectrum expands the previous IRTS and DIRBE spectra to 5.3 μm, and this blue EBL spectrum is consistent with the stellar spectrum. Dwek, Arendt, and Krennrich (2005a) tried to explain the high EBL brightness at 4.9 μm (Arendt & Dwek 2003) by the redshifted Hα emission from the first stars at $z > 6$, but this case is denied by our result. However, recent detailed theoretical studies (Cooray et al. 2012a; Fernandez et al. 2012; Yue et al. 2013) indicate that both of the expected brightness and fluctuations are 10-times or more fainter than the observed ones, although the spectral shape of excess emission and fluctuation is similar to the theoretical prediction. Cooray et al. (2012b) suggested a model to explain the EBL fluctuation by the diffuse intrahalo light of galaxies, but it looks difficult to explain the EBL excess. The exotic origins related to the dark matter and/or the dark energy seem to be

advantageous from the energetics point of view, but the theory concerning the origin of NIR EBL is not clear at present.

The origin of excess emission and fluctuation is still not clear, and new observations are highly expected to delineate their origin. The Cosmic Infrared Background ExpeRiment (CIBER) (Bock et al. 2006; Zemcov et al. 2013) will provide the spectrum of the sky at 0.75–1.8 μm with the Low Resolution Spectrometer (LRS) (Tsumura et al. 2010, 2013c) and fluctuation at 1.1 and 1.6 μm with the wide-field imagers (Bock et al. 2013) with a simultaneous observation of the absolute brightness of ZL with the Narrow-Band Spectrometer (NBS) (Korngut et al. 2013). An observation from outside the zodiacal cloud is also highly required to conduct an ideal observation of EBL without the strong ZL foreground. A small infrared telescope, EXo-Zodiacal Infrared Telescope (EXZIT), has been proposed as one of the instruments on a Solar Power Sail mission to Jupiter (Matsuura 2002). The measurement of NIR EBL at 5 au will be conducted in the 2020s.

This research is based on observations with AKARI, a JAXA project with the participation of ESA. This research is also based on significant contributions of the IRC team. We thank Mr. Arimatsu Ko (ISAS/JAXA) for discussion about the data reduction. The authors acknowledge support from Japan Society for the Promotion of Science, KAKENHI (grant numbers 21111004 and 24111717).

References

Aharonian, F., et al. 2006, Nature, 440, 1018
Aharonian, F., et al. 2007, A&A, 473, L25
Arendt, R. G., & Dwek, E. 2003, ApJ, 585, 305
Bernstein, R. A. 2007, ApJ, 666, 663
Bock, J., et al. 2006, New Astron. Rev., 50, 215
Bock, J., et al, 2013, ApJS, 207, 32
Cambŕesy, L., Reach, W. T., Beichman, C. A., & Jarrett, T. H. 2001, ApJ, 555, 563
Cohen, M. 1994, AJ, 107, 582
Cooray, A., et al. 2012b, Nature, 490, 514
Cooray, A., Gong, Y., Smidt, J., & Santos, M. G. 2012a, ApJ, 756, 92
Cooray, A., & Yoshida, N. 2004, MNRAS, 351, L71
Domínguez, A., et al. 2011, MNRAS, 410, 2556
Dwek, E., Arendt, R. G., & Krennrich, F. 2005a, ApJ, 635, 784
Dwek, E., Krennrich, F., & Arendt, R. G. 2005b, ApJ, 634, 155
Essey, W., & Kusenko, A. 2010, Astroparticle Phys., 33, 81
Fazio, G. G., et al. 2004a, ApJS, 154, 10
Fazio, G. G., et al. 2004b, ApJS, 154, 39
Fernandez, E. R., Iliev, I. T., Komatsu, E., & Shapiro, P. R. 2012, ApJ, 750, 20
Fernandez, E. R., & Komatsu, E. 2006, ApJ, 646, 703
Fernandez, E. R., Komatsu, E., Iliev, I. T., & Shapiro, P. R. 2010, ApJ, 710, 1089
Furniss, A., et al. 2013, ApJ, 768, L31
Girardi, L., Groenewegen, M. A. T., Hatziminaoglou, E., & da Costa, L. 2005, A&A, 436, 895
Hauser, M. G., et al. 1998, ApJ, 508, 25
Kashlinsky, A., Arendt, R. G., Ashby, M. L. N., Fazio, G. G., Mather, J., & Moseley, S. H. 2012, ApJ, 753, 63
Kashlinsky, A., Arendt, R. G., Mather, J., & Moseley, S. H. 2005, Nature, 438, 45
Kashlinsky, A., Arendt, R. G., Mather, J., & Moseley, S. H. 2007, ApJ, 654, L5
Keenan, R. C., Barger, A. J., Cowie, L. L., & Wang, W.-H. 2010, ApJ, 723, 40
Kelsall, T., et al. 1998, ApJ, 508, 44
Korngut, P. M., et al. 2013, ApJS, 207, 34
Levenson, L. R., Wright, E. L., & Johnson, B. D. 2007, ApJ, 666, 34
Madau, P., & Pozzetti, L. 2000, MNRAS, 312, L9
Madau, P., & Silk, J. 2005, MNRAS, 359, L37
Matsumoto, T., et al. 2005, ApJ, 626, 31
Matsumoto, T., et al. 2011, ApJ, 742, 124
Matsuoka, Y., Ienaka, N., Kawara, K., & Oyabu, S. 2011, ApJ, 736, 119
Matsuura, S. 2002, in Proc. Far-IR, Sub-mm & MM Detector Technology Workshop, ed. J. Wolf et al. NASA/CP-211408, i-04
Mattila, K., Lehtinen, K., Väisänen, P., von Appen-Gerhard, G., & Leinert, C. 2011, in IAU Symp. 284, The Spectral Energy Distribution of Galaxies, ed. R. J. Tuffs & C. C. Popescu (Cambridge, UK: Cambridge Universy Press), 429
Mazin, D., & Raue, M. 2007, A&A, 471, 439
Mii, H., & Totani, T. 2005, ApJ, 628, 873
Murakami, H., et al. 2007, PASJ, 59, S369
Ohyama, Y., et al. 2007, PASJ, 59, S411
Onaka, T., et al. 2007, PASJ, 59, S401
Pyo, J., Matsumoto, T., Jeong, W.-S., & Matsuura, S. 2012, ApJ, 760, 102
Raue, M., Kneiske, T., & Mazin, D. 2009, A&A, 498, 25
Salvaterra, R., & Ferrara, A. 2003, MNRAS, 339, 973
Sánchez-Conde, M. A., Paneque, D., Bloom, E., Prada, F., & Domínguez, A. 2009, Phys. Rev. D, 79, 123511
Santos, M. R., Bromm, V., & Kamionkowski, M. 2002, MNRAS, 336, 1082
Schlegel, D. J., Finkbeiner, D. P., & Davis, M. 1998, ApJ, 500, 525
Seon, K.-I., et al. 2011, ApJS, 196, 15
Thompson, R. I., Eisenstein, D., Fan, X., Rieke, M., & Kennicutt, R. C. 2007a, ApJ, 657, 669
Thompson, R. I., Eisenstein, D., Fan, X., Rieke, M., & Kennicutt, R. C. 2007b, ApJ, 666, 658
Totani, T., Yoshii, Y., Iwamuro, F., Maihara, T., & Motohara, K. 2001, ApJ, 550, L137
Tsumura, K., et al. 2010, ApJ, 719, 394
Tsumura, K., et al, 2013c, ApJS, 207, 33
Tsumura, K., Matsumoto, T., Matsuura, J., Pyo, S., Sakon, I., & Wada, T. 2013a, PASJ, 65, 119 (Paper I)
Tsumura, K., Matsumoto, T., Matsuura, S., Sakon, I., Tanaka, M., & Wada, T. 2013b, PASJ, 65, 120 (Paper II)
Tsumura, K., & Wada, T. 2011, PASJ, 63, 755
Uemizu, K., Bock, J. J., Kawada, M., Lange, A. E., Matsumoto, T., Watabe, T., & Yost, S. A. 1998, ApJ, 506, L15
Wright, E. L. 1998, ApJ, 496, 1
Yue, B., Ferrara, A., Salvaterra, R., & Chen, X. 2013, MNRAS, 431, 383
Zemcov, M., et al. 2013, ApJS, 207, 31